NASA TN D-1052

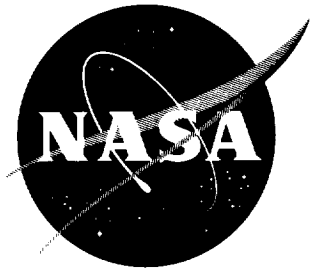

TECHNICAL NOTE
D-1052

RECOMBINATION OF HYDROGEN-AIR COMBUSTION PRODUCTS

IN AN EXHAUST NOZZLE

By Erwin A. Lezberg and Richard B. Lancashire

Lewis Research Center
Cleveland, Ohio

NATIONAL AERONAUTICS AND SPACE ADMINISTRATION

WASHINGTON August 1961

NATIONAL AERONAUTICS AND SPACE ADMINISTRATION

TECHNICAL NOTE D-1052

RECOMBINATION OF HYDROGEN-AIR COMBUSTION PRODUCTS IN AN EXHAUST NOZZLE

By Erwin A. Lezberg and Richard B. Lancashire

SUMMARY

Thrust losses due to the inability of dissociated combustion gases to recombine in exhaust nozzles are of primary interest for evaluating the performance of hypersonic ramjets. Some results for the expansion of hydrogen-air combustion products are described. Combustion air was preheated up to 3300° R to simulate high-Mach-number flight conditions. Static-temperature measurements using the line reversal method and wall static pressures were used to indicate the state of the gas during expansion.

Results indicated substantial departure from the shifting equilibrium curve beginning slightly downstream of the nozzle throat at stagnation pressures of 1.7 and 3.6 atmospheres. The results are compared with an approximate method for determining a freezing point using an overall rate equation for the oxidation of hydrogen.

INTRODUCTION

The high combustion temperatures encountered in jet engines for high-Mach-number flight lead to extensive dissociation of the combustion products. Since residence time in the exhaust nozzle is short, the combustion products - because of necessarily finite reaction rates - cannot follow the shifting equilibrium during expansion. If these recombination rates are slow, large thrust losses can occur. These losses are shown for a stoichiometric hydrogen-air system in figure 1 for the limiting cases of frozen and equilibrium expansions (ref. 1). The losses can be appreciably greater for hydrocarbons or systems involving condensable exhaust products.

A number of mathematical solutions have been recently applied to the expansion through a nozzle with reaction (refs. 2 to 6). These are essentially stepwise integral methods and thus far have involved only a single reaction. For fast computers, no limitations are seen to exist

for extending the methods to simultaneous reaction rates. The difficulty in applying these solutions is the present lack of knowledge of reaction rates, and relaxation rates in general, at the conditions of interest. Reaction-rate data obtained by measurement of concentration gradients in flat flames (refs. 7 to 12) and in shock tubes (e.g., ref. 13) may be applicable to the nozzle problem. The solutions must be checked, however, against actual measurements in a nozzle before any confidence can be established. The assumption that rates determined at conditions far removed from equilibrium can be applied to conditions near equilibrium leaves some doubts, since perturbations from a Maxwellian distribution may occur during radical recombination reactions (ref. 14).

Only a few experiments have been conducted to study recombination in a nozzle. In one of these experiments, where inlet conditions could be varied to produce flows varying from near-equilibrium to near-frozen flow, measurements were made for the recombination $2NO_2 \rightleftarrows N_2O_4$ (ref. 6). These showed good agreement with a complete solution of the flow.

The present work describes measurements of static pressures and temperatures for the hydrogen-air system in a convergent-divergent exhaust nozzle and is an extension of previous work described in reference 15. The operating conditions are designed to approximate ramjet flight at a Mach number of 6 at an altitude of about 100,000 feet. Fuel-air ratios up to 1.4 times stoichiometric were studied. The nozzle is conical with an exit-to-throat area ratio of 9.5:1 and a throat diameter of 3.08 inches.

The calibration procedure used for the line reversal pyrometer is described by Donald R. Buchele in appendix B, entitled "Calibration of Pyrometer with Arc Source."

TEST FACILITY

Air from the laboratory system was metered through a standard ASME orifice, heated, and passed through the test section, where fuel was introduced, burned, and the combustion products expanded through a supersonic nozzle. The flow was then cooled and ducted to the laboratory exhaust system. The facility is shown schematically in figure 2.

The storage-type heat exchanger (ref. 16) used to preheat the air consisted of a packed bed, 4 feet in diameter and 10.4 feet deep, insulated with refractory and insulating brick. The bed was packed with alumina balls 3/8 inch in diameter. It was heated by burning gasoline and air and passing the combustion products down through the bed. The bed was banked continuously at 1200° to 1500° F when not used for testing. During a test, the bed was heated to the desired operating temperature, after which the airflow through the bed was reversed. The heater will supply air at 3.6 atmospheres at a temperature up to 3300° R for periods up to 30 minutes.

The combustor and hydrogen-fuel injector (fig. 3) were both water-cooled. The injector was machined from a solid copper plate and had a blockage of 33 percent. Fuel was injected through 148 holes of 0.040-inch diameter facing downstream and drilled at 45° to the airflow direction. Fuel was taken from a bank of high-pressure cylinders, reduced in pressure to about 150 pounds per square inch gage, and metered through a standard ASME orifice. Flow was controlled by throttling downstream of the metering orifice.

The water-cooled nozzle had conical convergent and divergent sections joined by a circular arc at the throat and an exit-to-throat area ratio of 9.5:1. The contour and instrument locations are shown in figure 4.

Instrumentation

Static-pressure taps were drilled normal to the nozzle wall and were located spirally around the axis. Pressure taps were also located at the combustor inlet, outlet, and at the nozzle base. The pressures were read with the laboratory digital multiple-pressure recorder (ref. 17). Differential pressures at the metering orifices were read directly for air and through a mechanical pressure transmitter for the fuel. Water-orifice differential pressures and the fuel upstream-orifice pressure were measured with transducers. After each change in fuel flow, the flow was allowed to reach steady-state conditions before any data were taken by monitoring the nozzle static pressures on a mercury manometer board.

Temperatures of the cooling water, nozzle walls, air, and fuel at the metering orifices were measured with iron-constantan thermocouples.

Air temperature at the combustor inlet was measured with a platinum - platinum-13% rhodium cooled aspirated thermocouple probe. Two types were used during the course of this investigation: The first had a sonic nozzle insert (ref. 18); and the second, which was a stagnation cup with bleed holes for the aspirated gas, proved to have a longer lifetime in the high-temperature gas stream since the junction was not exposed to a high-velocity stream. Radiation and conduction errors were negligible for both probes. A recovery correction of 1.5 percent was applied to the sonic aspirated probe. All thermocouple outputs were read with a digital voltmeter in conjunction with the laboratory central data system (ref. 17). The inlet air temperature was also recorded on a strip-chart recorder.

Line reversal pyrometer. - The steady-state nozzle static temperatures at the port positions shown in figure 4 and the combustor-exit temperature profiles were measured with a self-balancing line reversal pyrometer (refs. 19 and 20) with a carbon-arc comparison source. Variation of the source intensity was accomplished by rotation of an optical

wedge in the light path. The optical diagram for the instrument is shown in figure 5. The calibration procedure is given in appendix B. Both the D lines of sodium centered at 5893 Å and the blue cesium line at 4553 Å were used for the reversal temperature measurements. The brightness temperature of the arc is higher at the lower wavelength and extended the range of the instrument to a higher temperature. Measurements could then be extended to the nozzle-inlet position. Sodium carbonate or cesium sulfate was introduced into the test section as a powder in a carrier gas stream through a water-cooled probe. The probe was mounted in an actuator at the combustor exit and could be traversed radially. The powder could thus be localized to a cross-sectional area of about 3/4-inch diameter at the nozzle inlet so that temperature profiles could be determined. The cesium sulfate used was somewhat hygroscopic (probably because of carbonate impurities), so that care was required in preventing moisture from entering the powder feeder (ref. 20). The powder was dried before use, and 1 percent of Celite was added. Cylinder nitrogen was passed through a dessicant cartridge and used as the carrier gas for the powder. Air was used with the sodium carbonate. The nozzle ports were closed with contoured plugs except at the station where the optical unit was mounted. Lenses at the nozzle ports were used to reduce the field of view.

Gas Sampling

Combustion-gas samples were withdrawn at a distance 15 inches downstream of the fuel injector and at various radial locations through a 0.020-inch-diameter water-cooled probe. A pressure ratio sufficient to obtain critical flow was maintained across the probe, and the samples were collected in 18-milliliter bottles.

Analysis for hydrogen, nitrogen, and oxygen was performed with a Perkin-Elmer gas chromatograph using argon as the carrier gas. The concentrations were determined by comparing peak heights with known samples.

Performance Calculations

Equilibrium flow. - The thermodynamic state following constant-pressure combustion or isentropic expansion of air to an assigned pressure was determined by a set of equations defining the equilibrium, conservation of mass, conservation of energy, partial pressures, and entropy. The successive approximation method was the same as that of reference 21. The thermodynamic data were taken from references 21 and 22. The calculations were programed for the UNIVAC 1103 computer.

The temperature and composition following the combustion process are found for the measured initial conditions of air and fuel temperature, pressure, fuel-air ratio, and heat loss to the fuel-injector cooling water. The entropy following the isentropic expansion must be equal to the entropy before the expansion:

$$S_o = \frac{1}{A} \sum_i \left[n_i \left(S_T^o \right)_i - Rn_i \ln p_i \right]_o$$

$$= \frac{1}{A} \sum_i \left[n_i \left(S_T^o \right)_i - Rn_i \ln p_i \right]_k \qquad (1)$$

(All symbols are defined in appendix A.) If A is taken as the number of formula weights divided by the static pressure,

$$p_i = n_i \qquad (2)$$

Equation (1) can then be written in terms of partial pressures alone. The solution is found by successive adjustment of the temperatures and partial pressures to satisfy equation (1) for an assigned static pressure lower than the initial pressure. The velocity at any point is determined from the energy equation,

$$U_k = \sqrt{2gJ(h_o - h_k)} \qquad (3)$$

where h_o is taken at the nozzle inlet. The nozzle area at any step of the expansion is determined from the continuity equation

$$\frac{A_k}{w} = \left(\frac{RT}{\bar{M} pU} \right)_k \qquad (4)$$

The throat area is determined by choosing the minimum from a pressure-area plot or simply as the minimum area determined from the stepwise calculation, using an initially small pressure step size.

Frozen flow. - The composition is assumed frozen at the nozzle inlet following equilibrium constant-pressure combustion. The partial pressures at the k^{th} step of the expansion are

$$(p_i)_k = \frac{p_k}{p_o} (p_i)_o \qquad (5)$$

and the total entropy per equivalent formula weight of reactant is

$$S_k = S_o - R \ln \frac{p_k}{p_o} \tag{6}$$

where S_o is given by equation (1). The temperature is determined by satisfying (1) for temperature, where the n_j's are the initial values following combustion.

Partially frozen flow. - The equilibrium calculations are followed to the step corresponding to the assumed freezing point. The composition is then assumed fixed, and the calculation is resumed as in the case of frozen flow but using the values of mole fraction at the freezing point as initial conditions. The initial enthalpy in equation (3) must continue to be the value at the combustor.

RESULTS AND DISCUSSION

Nozzle Calibration

A cold-flow static-pressure calibration of the nozzle was made to determine the equivalent area ratio of the nozzle for the one-dimensional expansion of an ideal gas with $\gamma = 1.4$. Dry air was used during the test. The boundary-layer displacement thickness was computed by the method of reference 23, described in appendix C. Calculated displacement thicknesses for cold air, hot air, and stoichiometric combustion products are shown in figure 6. The equivalent area ratios from the cold-flow calibration and the area ratios corrected for the cold-air boundary-layer displacement thickness are shown in figure 7. The symbols show the area ratios at the static tap locations representing source flow and are the ratio of the spherical cap area to the sonic flow area. The sonic flow area was computed from the measured cold-air mass flow, total pressure, and temperature. Using this value for the throat area, the comparison to the calibration data corrected for boundary layer is quite good.

Air-temperature measurements. - Radial air-temperature profiles were measured at the combustor outlet with the line reversal method using the tungsten lamp source and sodium tracer. The temperature was found to be flat within 120° F to 1 inch from the wall at about 3200° R. The average temperature was within 30° F of the thermocouple measurement. A fluctuation at a frequency of 3 to 4 cycles per second in the air-temperature measurements was sensed by the aspirating thermocouple. The magnitude of the fluctuation was of the order of ±100° F near the wall but was considerably reduced near the center of the duct. The magnitude of the fluctuations was also considerably reduced at the lower inlet pressure of 1.7 atmospheres.

Expansion of heated air. - A static-pressure profile for air at 3300° R is shown in figure 8, together with the calculated equilibrium and frozen vibration profiles. The inlet temperature has been corrected for the cooling loss to the fuel injector. The equilibrium and frozen pressure ratios are evaluated at the equivalent one-dimensional area ratios. The area ratios at the pressure tap locations have been corrected for the change in boundary-layer displacement thickness from the cold-flow to heated-air conditions. The dotted line is plotted through the data by using the method of least squares and has a standard deviation about this line of 0.46 percent. It appears to indicate a lag in relaxation of vibrational energy. A discontinuity in the profile at an area ratio of 2.1 was typical of all the data including the calibration and was possibly due to a discontinuity in the nozzle contour.

Combustion-gas samples. - A comparison of the measured and calculated equilibrium composition of the samples plotted against sample equivalence ratio is shown in figure 9 and is presented in table I. Analysis was on a dry basis for hydrogen, nitrogen, and oxygen. Argon was used as the carrier gas and thus does not show up in the analysis, but was computed as 1.21 percent of the nitrogen present in the sample.

Nitric oxide was assumed to be oxidized in the sample to NO_2 and to be absorbed in the water present as the acids. It would presumably be lost by absorption in the desiccant used for drying the samples or as liquid remaining in the sample bottles. Corrections to the sample composition for NO were made on the basis of the mole fraction present at equilibrium and the oxygen in the sample corrected for oxidation of NO to NO_2.

The water vapor formed during combustion was computed as

$$n_{H_2O} = 2\,\Delta n_{O_2} \tag{7}$$

where the initial number of moles of oxygen is given as

$$n_{O_{2,o}} = \frac{1}{3.76}\left(n_{N_{2,s}} + \frac{1}{2}\,n_{NO_{eq}}\right) \tag{8}$$

and the final number of moles as

$$n_{O_2} = n_{O_{2,s}} + \frac{1}{2}\,n_{NO_{eq}} \tag{9}$$

The equilibrium compositions were computed from the data of references 21 and 22 at the same pressure, overall equivalence ratio, and combustion temperature as the sample. If the hydroxyl radical is assumed to recombine to form water, the compositions are in fairly good agreement and

indicate that there are no large deviations from equilibrium at the nozzle inlet.

The compositions are also given in table I at various radial sampling positions. It was not possible to hold conditions constant during a radial survey because of the time involved in sampling and changing sample bottles; however, there are no pronounced discrepancies between the overall and sample equivalence ratios at any radial position.

Combustor temperature profiles. - Radial temperature profiles at the combustor exit are shown in figure 10. These measurements were made by reversal of the 4553 Å line of cesium while injecting cesium sulfate powder through a traversing probe. Superimposed on figure 10(a) is a sketch of the fuel injector showing its position relative to the powder-injecting probe. The asymmetry of the profile may be caused by a few plugged orifices and presumably would be averaged-out over other angular positions. Since the injector orifices were sized for critical flow at stoichiometric fuel flow at 3.6 atmospheres burner pressure, the distribution and mixing would be expected to be poorer at low fuel flows. This is evident from the profile shown for an equivalence ratio of 0.644 at 1.9 atmospheres in figure 10(b). The theoretical combustion temperature considering only cooling loss to the fuel injector is noted on each profile and compares quite well with the measured temperature near the center of the duct for equivalence ratios near stoichiometric. The theoretical combustion temperature corrected for cooling loss to the combustor wall has been compared with the area-weighted average from the profiles and also agrees reasonably well for all the profiles. It appears, then, that the shape of the profiles for near-stoichiometric mixtures is due principally to heat transfer to the walls.

Expansion of Hydrogen-Air Combustion Products

Static-temperature measurement. - Sodium D-line reversal temperature measurements at an area ratio of 1.23 for pressures of 3.6 and 1.7 atmospheres and air temperatures from 2880° to 3185° R are plotted in figure 11 as a function of equivalence ratio. The calculated equilibrium and frozen static temperatures are shown for comparison. The temperatures essentially follow the equilibrium curve at the higher pressure and show some departure from the equilibrium line at the lower pressure for close-to-stoichiometric mixtures. For lean mixtures the higher-than-equilibrium temperatures can be attributed to weighting by the reversal instrument. Since temperature zones higher than the calculated mean combustion temperatures exist because of poor fuel distribution and mixing, spreading of the injected tracer or sodium salts contaminating the air stream will tend to weight the indicated reversal strongly toward the high-temperature peaks. Another cause of this weighting is the effect of the air-temperature fluctuations noted earlier. Changes in mass flow to choke

the nozzle accompanying the air-temperature fluctuations produce changes in fuel-air ratio. This either accentuates or diminishes the combustion-temperature changes, depending on whether the mixture is leaner or richer than stoichiometric. The earlier results of this work reported in reference 14 were more subject to error from this source, since the frequency response of the instrument used was limited by a 0.5-second lag of the tungsten filament. The frequency response of the modified reversal instrument was limited to about 4 cycles per second by the servomotor that drives the optical wedge. This, however, was fast enough to respond to the changes just noted, so that averaging over the recorder fluctuations yielded the correct average temperature. Further errors at lean mixtures may be due to small-scale inhomogeneities in mixing that could not be resolved because of the limiting time response or the spreading of the sodium tracer stream.

Figure 12 shows the measured reversal temperatures at an area ratio of 1.77. Here, the deviation from the equilibrium curve is quite pronounced for near-stoichiometric mixtures. The data at the lower pressure of 1.7 atmospheres indicate somewhat greater departure. The weighting toward high temperatures at lean equivalence ratios is also apparent at this location.

The static temperatures are plotted in figure 13 as a function of area ratio at an equivalence ratio of 1. The area ratios for the data points were negligibly affected by the boundary-layer corrections and are taken from the cold-flow calibration at the axis of the optical path. Static temperatures at the last measuring station, where $A/A^* = 5.14$, could not be measured because they were below the range of the instrument (2955° R). The departure from the equilibrium curve occurs between the first and second measuring stations at 3.6 atmospheres, and somewhat before the first measuring station at 1.7 atmospheres.

Pressure measurements. - Static-pressure profiles for hydrogen-air combustion products are shown in figure 14(a) at an equivalence ratio of 1.04, combustion temperature of 5230° R, and a total pressure of 3.6 atmospheres. The area ratios at the static tap locations have been corrected for change in boundary-layer displacement thickness for a frozen boundary layer at an equivalence ratio of about 1.0. A curve has been fitted to the data by the method of least squares. The data have a standard deviation about this curve of 0.42 percent and indicate departure from the equilibrium line slightly downstream of the throat.

The pressure ratios at the last static tap location are shown plotted in figure 14(b) as a function of equivalence ratio. The frozen line has been corrected for boundary-layer losses and appears as the dashed line. The boundary layer was computed at equivalence ratios of 1.0, 0.6, and for heated air alone; and the correction was interpolated for intermediate values. Since the boundary-layer corrections depend very strongly on the

ratio of wall to free-stream enthalpies, the corrections would be sensitive to nonuniform free-stream properties. At lean equivalence ratios, where the profiles indicated higher temperatures nearer the walls due to uneven fuel distribution through the injector, the free-stream to wall temperature ratios higher than theoretical would result in a smaller displacement thickness; and hence the actual correction to the area ratio should be larger. The data would then follow the corrected frozen line fairly closely over the complete equivalence ratio range.

Calculation of the apparent freezing point. - Recent work at this laboratory (ref. 12) on gas sampling downstream of lean, flat, hydrogen-air flames has yielded a rate equation for an overall reaction:

$$H_2 + \frac{1}{2} O_2 \underset{k_D}{\overset{k_R}{\rightleftharpoons}} H_2O \tag{10}$$

A rate equation for the decay of hydrogen downstream of a flat flame was found to be best described by

$$-\frac{d[H_2]}{dt} = 1.7\times10^{10}[H_2]^{3/2}[O_2]e^{-\frac{8100}{RT}} \tag{11}$$

This expression probably represents a lower limit, since diffusion was neglected in fitting the data. Since the concentrations of hydrogen downstream of these flames are in large excess of equilibrium, the rate equation is essentially a recombination rate and may be used to satisfy the Bray criterion (ref. 3) for a freezing point. The Bray freezing point is defined for the dissociation and three-body recombination of a diatomic molecule, where the net rate of reaction at equilibrium is approximately equal to the rate of dissociation. Since $r_D \cong r_R$, where departures from equilibrium begin to occur, the Bray criterion for the freezing point may be written as

$$-\frac{d\alpha}{dt} = Kr_R \tag{12}$$

where K is about unity.

At equilibrium, the net rate of change of any species may be written as

$$\frac{d[\ ]_i}{dt} = \frac{d[\ ]_{i,eq}}{dt} - \frac{d[\ ]_i}{dt}(\rho) \tag{13}$$

where the concentrations are given by

$$[\ ]_i = X_i \frac{\rho}{\bar{M}} \tag{14}$$

Equation (13) states that the net rate due to reaction alone equals the total rate minus the change in partial molar density due to the expansion. The concentration due to density change will be

$$[\ ]\ f(\rho) = \frac{X_{i,o}\ \rho}{\bar{M}_o} \tag{15}$$

The density is taken from the equilibrium flow calculations, since the reaction will affect the flow appreciably. A graphical solution of equations (11) and (13) should give the freezing point. If the overall reaction given by equation (10) is considered, the net rate of change of $[H_2O]$ is determined from the equilibrium calculation as

$$\frac{d[H_2O]}{dt} = U \frac{d}{dx} \left\{ [H_2O]_{eq} - [H_2O]_o f(\rho) \right\} \tag{16}$$

Equations (11) and (16) are plotted in figure 15 against distance for stoichiometric mixtures at 3.6 and 1.7 atmospheres. A freezing point is indicated at an area ratio of 1.02 downstream of the throat at 3.6 atmospheres and at an area ratio of 1.07 upstream of the throat for a pressure of 1.7 atmospheres. At stagnation pressures of 3.6 and 1.7 atmospheres, freezing points were assumed at intervals in the vicinity of the throat, and the flow was calculated with frozen concentration assumed downstream of the point. The best fit of these calculations to the data was a freezing point at an area ratio of 1.1 for the higher pressure, and at an area ratio of 1.05 for the lower pressure. The computed temperatures are shown as dashed lines in figure 13. The computed pressures are shown by the square symbols in figure 14(a). Relating these apparent freezing points back to the rate equation (11) yields a rate constant of 2.3×10^{10} for the higher pressure and 6.4×10^{10} for the lower pressure. In view of the uncertainty in determining the rate equation in the work on flat flames, and in extrapolating it to the nozzle flow conditions, the agreement is probably better than should be expected. The pressure data (fig. 14(a)) show good agreement with the calculations based on Bray's approximation. For a more adequate comparison with the data, however, an exact calculation of the flow with reaction is needed.

SUMMARY OF RESULTS

Departures from chemical equilibrium have been observed for the expansion of near-stoichiometric hydrogen-air combustion products through a convergent-divergent exhaust nozzle.

1. Static-temperature measurements show a nonequilibrium condition near the throat followed by a rapid decrease in temperature toward the frozen composition line. These measurements at 3.6 and 1.7 atmospheres indicated a greater degree of recombination at the higher total pressure.

2. Wall static-pressure measurements also indicate a nonequilibrium condition slightly downstream of the throat for a total pressure of 3.6 atmospheres; it was shown that the data approximated an expansion corresponding to one in which the composition had frozen at an area ratio of 1.1 downstream of the throat.

3. The application of an approximate freezing criterion to an overall reaction rate for the oxidation of hydrogen and air predicts freezing of the composition in the vicinity of the nozzle throat.

Lewis Research Center
National Aeronautics and Space Administration
Cleveland, Ohio, June 13, 1961

APPENDIX A

SYMBOLS

A	cross-sectional area of nozzle, number of equivalent formula weights
a	velocity of sound
C_1, C_2	Planck's radiation constants
f	function
g	gravitational constant
H	form factor, δ^*/θ
H_i	incompressible form factor
$H_{i,fp}$	flat-plate incompressible form factor = 1.3
h	enthalpy per unit mass
J	mechanical equivalent of heat
K	constant in eq. (12)
k	reaction-rate constant
M	Mach number
$\bar{M}$	mean molecular weight
N_λ	monochromatic areal intensity
n	number of moles
Pr	Prandtl number
p	static pressure
p_i	partial pressure of the i^{th} species
R	universal gas constant
r	reaction rate

E-1246

S	entropy per mole
T	temperature
$\overline{T}$	average temperature
t	time
U	velocity
w	mass-flow rate
X	mole fraction
x	axial distance from nozzle inlet
y	distance normal to axis of nozzle
α	fraction dissociated
γ	ratio of specific heats
δ^*	displacement thickness
ϵ	emissivity
θ	momentum thickness
λ	wavelength
ν	kinematic viscosity
ρ	density
τ	optical transmission factor
φ	equivalence ratio

Subscripts:

C	cooled
D	dissociation
e	free stream
eq	equilibrium

g	combustion gas
i	i^{th} species
k	k^{th} step in expansion
o	stagnation state, initial conditions
R	recombination
ref	reference
s	sample
T	temperature
tr	transformed quantity
w	wall

Superscripts:

0	standard state
*	conditions at sonic throat

APPENDIX B

CALIBRATION OF PYROMETER WITH ARC SOURCE

By Donald Buchele

The illumination system of the pyrometer with a carbon arc source is shown in figure 5. The tungsten lamp source of reference 19 has been replaced by a pair of circular absorption wedges, which are illuminated by a carbon arc image focused on them by a condensing lens. The logarithm of the wedge transmission factor varies from 0 to 3 and is linear with the angle of rotation. Wedge position is transmitted by a potentiometer. Self-balancing operation is obtained by rotation of one of the wedges. The other wedge is stationary and is used at the position of maximum transmission; it has an optical density increasing counterclockwise, opposite to that of the other wedge. This provides a large area of uniform transmission for any position of the movable wedge. An interference filter and an air-cooled Plexiglas window are necessary to avoid excessive wedge temperature. Bandwidth of the interference filter is 3 percent of the wavelength.

The intensity N_λ at the gas location and the corresponding temperature for the spectral wavelength used are determined by a calibration. Under blackbody conditions, the intensity of a radiating source is given by Planck's equation:

$$N_{\lambda,b} = C_1\lambda^{-5}\left(e^{C_2/\lambda T_b} - 1\right)^{-1} \tag{B1}$$

where T_b is the temperature of the blackbody. For nonblackbody conditions, including an emissivity ϵ_λ and an optical transmission factor τ_λ between the radiating source and the point of observation, the observed monochromatic areal intensity is

$$N_{\lambda,a} = \tau_\lambda\epsilon_\lambda N_{\lambda,b} = C_1\lambda^{-5}\left(e^{C_2/\lambda T_a} - 1\right)^{-1} \tag{B2}$$

where T_a is an apparent temperature corresponding to the observed radiation intensity. Equations (B1) and (B2) are the basic equations of calibration.

In the optical path of figure 5 radiation from the arc is transmitted by three groups of elements: τ_1, τ_2, and τ_3; τ_1 includes all optical elements except τ_2, the interference filter; and τ_3 is the nozzle or test-section window optics. Using the Wien approximation to Planck's equation, N_λ at the gas location is

$$N_{\lambda,a} = C_1\epsilon_\lambda\tau_{\lambda_1}\tau_{\lambda_2}\tau_{\lambda_3}\lambda^{-5}e^{-C_2/\lambda T_b} = C_1\lambda^{-5}e^{-C_2/\lambda T_a} \tag{B3}$$

where T_b is the thermal temperature of the arc and T_a is the apparent temperature of the arc observed at the gas location. An optical pyrometer sighted on the arc crater indicates a temperature T_c at the pyrometer wavelength λ_p and arc emissivity ϵ_p. The intensity is

$$N_{p,c} = C_1 \epsilon_p \lambda_p^{-5} e^{-C_2/\lambda_p T_b} = C_1 \lambda_p^{-5} e^{-C_2/\lambda_p T_c} \tag{B4}$$

Letting $\epsilon_\lambda = \epsilon_p$ (the arc is assumed to be a gray-body radiator), equations (B3) and (B4) combine to yield

$$\frac{1}{T_a} = \frac{1}{T_b} + \frac{(\lambda_p - \lambda)}{C_2} \ln \epsilon_p - \frac{\lambda}{C_2} \ln \tau_{\lambda,1} \tau_{\lambda,2} \tau_{\lambda,3} \tag{B5}$$

This is the calibration equation. Wavelength λ is of the spectral line; λ_p is of the pyrometer, 0.65 micron. The emissivity of the arc is taken as 0.98 from reference 24. The transmission factors $\tau_{\lambda,1}$ and $\tau_{\lambda,3}$ vary gradually with wavelength. They are measured photoelectrically in the vicinity of the spectral line by using only the light transmitted by the interference filter. The transmission factor $\tau_{\lambda,2}$ of the interference filter is measured with a spectrometer using a bandwidth of 0.0020 micron or less at the wavelength of the spectral line. A further correction in the case of the double-pass system for the transmission of the optics and reflector on the reflector side of the light path is made as in appendixes B and C of reference 18. The loop transmission factor resulting from reflection of light from the tungsten lamp filament would, however, be different in the case of the arc unit. A reflection factor of 0.12 is produced by the glass surfaces of the optical wedge, although the arc itself does not reflect. Consequently, a special value of τ_1 used in the loop transmission term includes only the optics between the wedge and the gas. The correction for the loop transmission was found to be negligible for these measurements and was subsequently omitted.

APPENDIX C

BOUNDARY-LAYER CORRECTIONS

Momentum losses due to heat transfer to the cooled nozzle walls have been calculated by using the method of reference 23, which was modified to include the effect of specific heat ratios other than 1.4. The method involves the momentum integral and moment-of-momentum equations as simplified by using Stewartson's transformation. It assumes uniform and reversible free-stream properties with irreversible flow in the boundary layer.

The quantity generally accepted as the best correction to apply to a flow is the boundary-layer displacement thickness δ^*. It cannot be determined directly but may be calculated by using the relation

$$H = \frac{\delta^*}{\theta} \tag{C1}$$

where θ is the boundary-layer momentum thickness and H is the form factor. These two quantities are determined with the transformed momentum and moment-of-momentum integral equations, respectively. Modified from reference 23, the equations are:

$$\theta_{tr}^{1.2155} = \left(\frac{1}{\left(\frac{a_o}{\nu_o}\right)^{0.2155} M_e^{B+0.2155}\, y^{1.2155}} \right) \cdot \left\{ \left[\theta_{tr}^{1.2155}\, M_e^{B+0.2155} \left(\frac{a_o}{\nu_o}\right)^{0.2155} y^{1.2155} \right]_{x=0} + 0.01173 \int_0^x \frac{M_e^B \left(\frac{T_e}{T_{ref}}\right)^{0.732} y^{1.2155}}{\left(\frac{T_o}{T_e}\right)^D} dx \right\} \tag{C2}$$

and

$$\frac{dH_i}{dx} = -\frac{1}{M_e}\frac{dM_e}{dx}\left[\frac{H_i(H_i+1)^2(H_i-1)}{2}\right]\left\{1+\left(\frac{h_w}{h_o}-1\right)\right.$$

$$\left.\cdot\left[\frac{2H_{i,fp}}{H_i+1}\frac{1}{2}\left(\frac{H_i+1}{H_i-1}\right)\left(\frac{H_{i,fp}-1}{H_{i,fp}+3}\right)\right]\right\} - 0.03\,H_i(H_i^2-1)\frac{A}{\theta_{tr}} \qquad (C3)$$

where

$$A = 0.123\,e^{-1.561\,H_i}\left(\frac{M_e a_o \theta_{tr}}{\nu_o}\right)^{-0.268}\left(\frac{T_e}{T_{ref}}\right)^{0.732}\left(\frac{T_e}{T_o}\right)^{D} \qquad (C4)$$

$$B = 4.2 + 1.58\left(\frac{h_w}{h_o}-1\right) \qquad (C5)$$

and

$$D = 4.206\,\frac{(0.936\,\gamma - 1)}{\gamma - 1} \qquad (C6)$$

The quantities at the reference conditions are determined with the equation

$$\frac{h_{ref}}{h_e} = 0.5\left(\frac{h_w}{h_o}+1\right) + 0.11(\gamma-1)\,(Pr)_{ref}^{1/3}\,M_e^2 \qquad (C7)$$

The enthalpies were computed with the data of reference 21. The calculations were made with the assumption that the equilibrium composition at the combustor exit was frozen throughout the nozzle. Calculations for equilibrium composition throughout the nozzle were not made, because it was believed that the differences between a frozen boundary layer with a frozen free stream and one with an equilibrium free stream would be very small since N_2 makes the largest contribution to the specific heat of the mixture.

Physically, transformed quantities (subscript "tr") refer to a non-insulated boundary layer at a Mach number of zero and include the variation of density with temperature. For boundary layers over insulated surfaces, and where Prandtl number equals 1, the transformed and incompressible (subscript "i") quantities are identical.

The compressible momentum thickness is obtained using the relation

$$\theta = \theta_{tr}\left(1 + \frac{\gamma - 1}{2} M_e^2\right)^{\frac{\gamma+1}{2(\gamma-1)}} = \theta_{tr}\left(\frac{T_o}{T_e}\right)^{\frac{\gamma+1}{2(\gamma-1)}} \qquad (C8)$$

The relation between the compressible and incompressible form factors is as follows

$$H = \left(\frac{T_o}{T_e}\right)\left[(H_i + 1) + \left(\frac{h_w}{h_o}\right) - 1\ H_{i,fp}\right] - 1 \qquad (C9)$$

A program was set up on the IBM 704 computer to solve equations (C1) to (C9). The output from this program yielded the boundary-layer displacement thickness δ^* as a function of x. The solution of equation (C3) required the value of H_i at $x = 0$. This starting value of H_i was determined by first evaluating the compressible form factor H at Mach 0 using the tabulated integrals of reference 25. The incompressible form factor H_i at Mach 0 was then determined from equation (C9). Since the evaluation of H_i in this manner included the effects of Prandtl number and heat transfer, it was believed to be a better approximation than the use of the flat-plate value of 1.3. The values of H_i were of the order of 1.2 for both the heated air and combustion cases.

The values of the transformed momentum thickness at $x = 0$ were calculated by the flat-plate analysis of reference 23.

Referring to figure 6, note that a negative displacement thickness exists over the throat region for the heated air and combustion cases. Negative displacement thicknesses are to be expected where the thermal boundary layer is much thicker than the velocity layer, because higher densities in the boundary layer relative to those in the free stream result in higher boundary-layer values of mass flow per unit area. Physically, this fact means that the flow area is greater in this region than the calibrated area.

REFERENCES

1. Reynolds, T. W.: Effect of Dissociation on Exhaust-Nozzle Performance. NACA RM E58C25, 1958.

2. Reynolds, Thaine W., and Baldwin, Lionel V.: One-Dimensional Flow with Chemical Reaction in Nozzle Expansion. Paper presented at Symposium on Thermodynamics of Jet and Rocket Prop., A.I.Ch.E., Kansas City, May 17-20, 1959.

3. Bray, K. N. C.: Departure from Dissociation Equilibrium in a Hypersonic Nozzle. Rep. 19,983, British ARC, Mar. 17, 1958.

4. Hall, J. Gordon: Dissociation Nonequilibrium in Hypersonic Nozzle Flow. Preprint 7, A.I.Ch.E., 1959.

5. Heims, Steve P.: Effect of Oxygen Recombination on One-Dimensional Flow at High Mach Numbers. NACA TN 4144, 1958.

6. Wegener, Peter P.: Supersonic Nozzle Flow with a Reacting Gas Mixture. The Phys. of Fluids, vol. 2, no. 3, May-June 1959, pp. 264-275.

7. Fenimore, C. P., and Jones, G. W.: The Water-Catalyzed Oxidation of Carbon Monoxide by Oxygen at High Temperature. Jour. Phys. Chem., vol. 61, no. 5, May 1957, pp. 651-654.

8. Kaskan, W. E.: Hydroxyl Concentrations in Rich Hydrogen-Air Flames Held on Porous Burners. Combustion and Flame, vol. 2, no. 3, Sept. 1958, pp. 229-243.

9. Kaskan, W. E.: The Concentration of Hydroxyl and of Oxygen Atoms in Gases from Lean Hydrogen Air Flames. Combustion and Flame, vol. 2, no. 3, Sept. 1958, pp. 286-304.

10. Friedman, R., and Nugent, R. G.: Flame Structure Studies, IV - Pre-Mixed Carbon Monoxide Combustion. Seventh Symposium (International) on Combustion, Butterworths Sci. Pub., 1951, pp. 311-314; discussion, pp. 314-316.

11. Westenberg, A. A., and Fristrom, R. M.: Chemical Kinetic Considerations. CM-974, Appl. Phys. Lab., Johns Hopkins Univ., June 1960.

12. Fine, Burton: Kinetics of Hydrogen Oxidation Downstream of Lean Propane and Hydrogen Flames. Jour. Phys. Chem., vol. 65, no. 3, Mar. 1961, pp. 414-417.

13. Bauer, S. H., Schott, G. L., and Duff, R. E.: Kinetic Studies of Hydroxyl Radicals in Shock Waves. I - The Decomposition of Water Between 2400° and 3200° K. Jour. Chem. Phys., vol. 28, no. 6, June 1958, pp. 1089-1096.

14. Mahan, Bruce H.: Perturbation of Molecular Distribution Functions by Chemical Reaction. Jour. Chem. Phys., vol. 32, no. 2, Feb. 1960, pp. 362-364.

15. Lezberg, Erwin A., and Lancashire, Richard B.: Expansion of Hydrogen-Air Combustion Products Through a Supersonic Exhaust Nozzle; Measurements of Static-Pressure and Temperature Profiles. "Combustion and Propulsion" - Fourth AGARD Colloquium. Pergamon Press, 1961.

16. Lancashire, Richard B., Lezberg, Erwin A., and Morris, James F.: Experimental Results of a Heat-Transfer Study from a Full-Scale Pebble-Bed Heater. NASA TN D-265, 196C.

17. Staff of the Lewis Laboratory: Central Automatic Data Processing System. NACA TN 4212, 1958.

18. Glawe, George E.: A High Temperature Combination Sonic Aspirated Thermocouple and Total Pressure Probe. Jet Prop., vol. 27, no. 5, May 1957, pp. 543-544.

19. Buchele, Donald: A Self-Balancing Line-Reversal Pyrometer. NACA TN 3656, 1956.

20. Buchele, D.: A Self-Balancing Line Reversal Pyrometer. Paper presented at Fourth Symposium on Temperature, Its Measurement and Control in Sci. and Industry, Columbus (Ohio), Mar. 27-31, 1961.

21. Gordon, Sanford, Zeleznik, Frank J., and Huff, Vearl N.: A General Method for Automatic Computation of Equilibrium Compositions and Theoretical Rocket Performance of Propellants. NASA TN D-132, 1959.

22. Hilsenrath, Joseph, et al.: Tables of Thermal Properties of Gases. Cir. 564, U.S. Dept. Commerce, NBS, Nov. 1, 1955.

23. Reshotko, Eli, and Tucker, Maurice: Approximate Calculation of the Compressible Turbulent Boundary Layer with Heat Transfer and Arbitrary Pressure Gradient. NACA TN 4154, 1957.

24. Null, M. R., and Lozier, W. W.: Measurement of Reflectance and Emissivity of Graphite at Arc Temperature with a Carbon Arc Image Furnace. Jour. Appl. Phys., vol. 29, no. 11, Nov. 1958, p. 1605.

25. Bartz, D. R.: An Approximate Solution of Compressible Turbulent Boundary-Layer Development and Convective Heat Transfer in Convergent-Divergent Nozzles. Trans. ASME, vol. 27, no. 8, Nov. 1955, pp. 1235-1245.

TABLE I. - COMBUSTION-GAS SAMPLES

[p_o, 3.6 atm.]

	Combustion temperature, T, °R	Equivalence ratio, φ	Radial probe position, in.	Gas-composition mole fraction, X_i				
				X_{N_2}	X_{O_2}	X_{H_2}	X_{H_2O}	$X_{OH_{eq}}$
(eq)*	5076	1.16		0.605	0.0034	0.064	0.294	0.0158
(s)**		1.09	6	.618	.0021	.044	.326	
eq	5197	1.075		.614	.0076	.052	.280	.0224
s		1.14	6	.611	.0038	.054	.318	
eq	4694	.577		.691	.0684	.0040	.200	.0158
s		.666	$3\frac{1}{2}$	.674	.0586	.0004	.243	
eq	5237	1.16		.599	.0050	.0697	.280	.0211
s		.870	$3\frac{1}{2}$	.660	.0269	.0009	.307	
eq	5236	1.02		.616	.0096	.0491	.274	.0245
s		.966	$3\frac{1}{2}$	.636	.0164	.0226	.308	
eq	5168	.915		.637	.0182	.030	.263	.0259
s		1.01	0	.627	.0110	.030	.312	
eq	5188	.945		.632	.0157	.034	.266	.0257
s		1.01	$\frac{1}{2}$	.626	.0157	.034	.306	
eq	5129	.875		.644	.0220	.0246	.259	.0255
s		.985	1	.631	.0124	.0273	.311	
eq	5144	.891		.641	.0204	.0267	.261	.0257
s		.920	2	.641	.021	.0172	.301	

*Temperatures and composition calculated for equilibrium combustion at overall equivalence ratio.

**Composition and equivalence ratio calculated from sample.

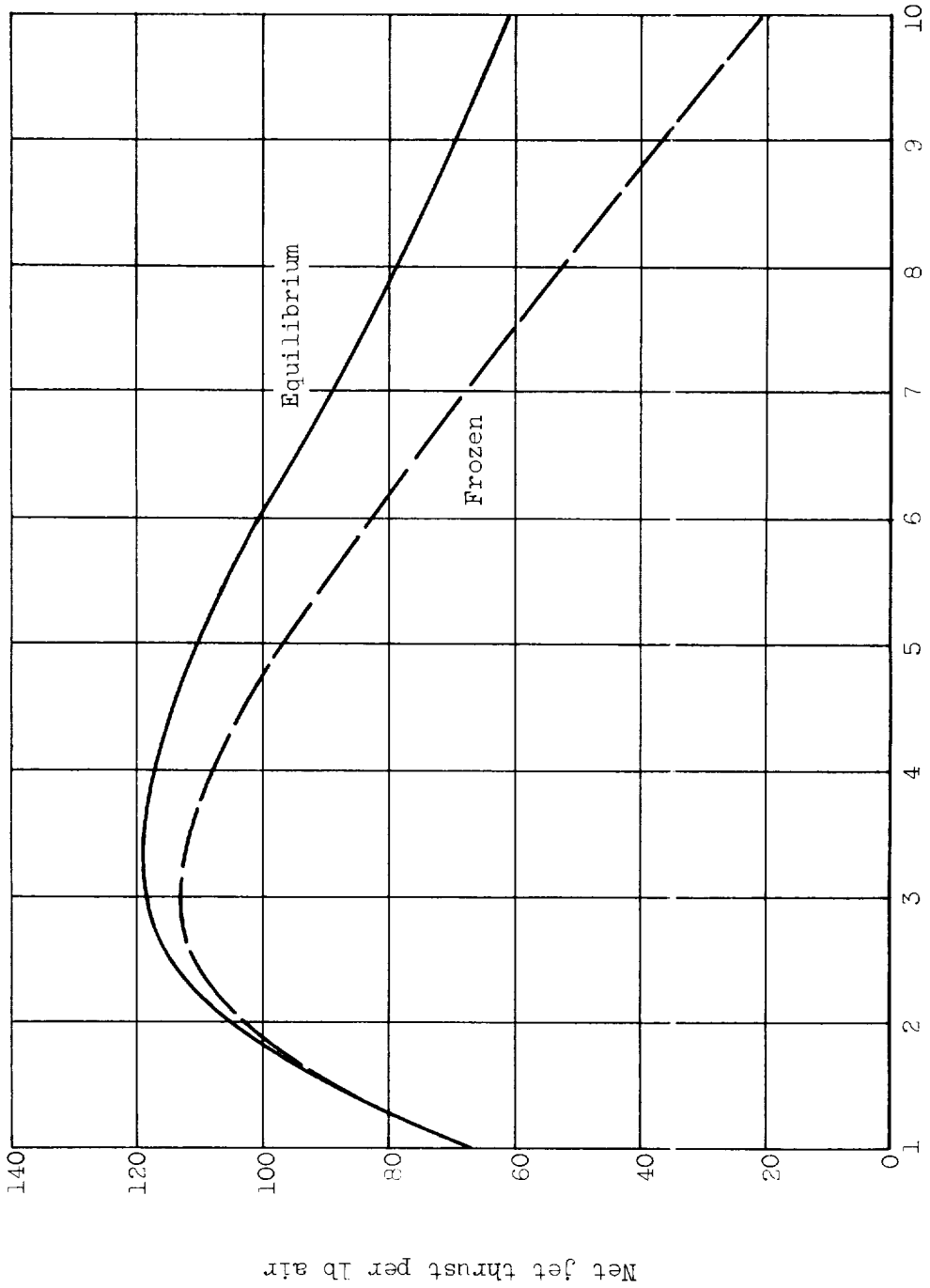

Figure 1. - Ramjet net jet thrust for stoichiometric hydrogen-air combustion products.

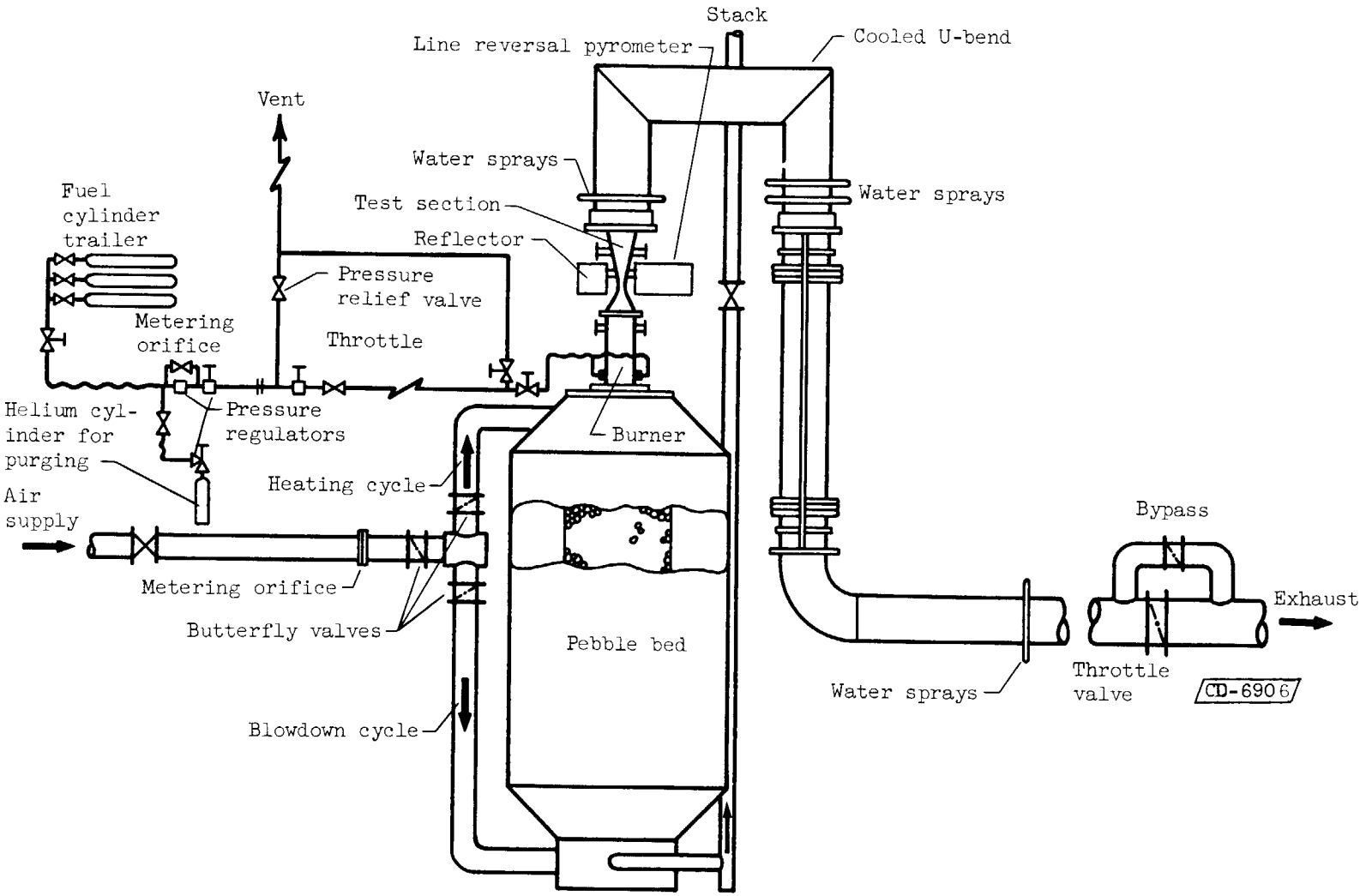

Figure 2. - Nozzle test facility.

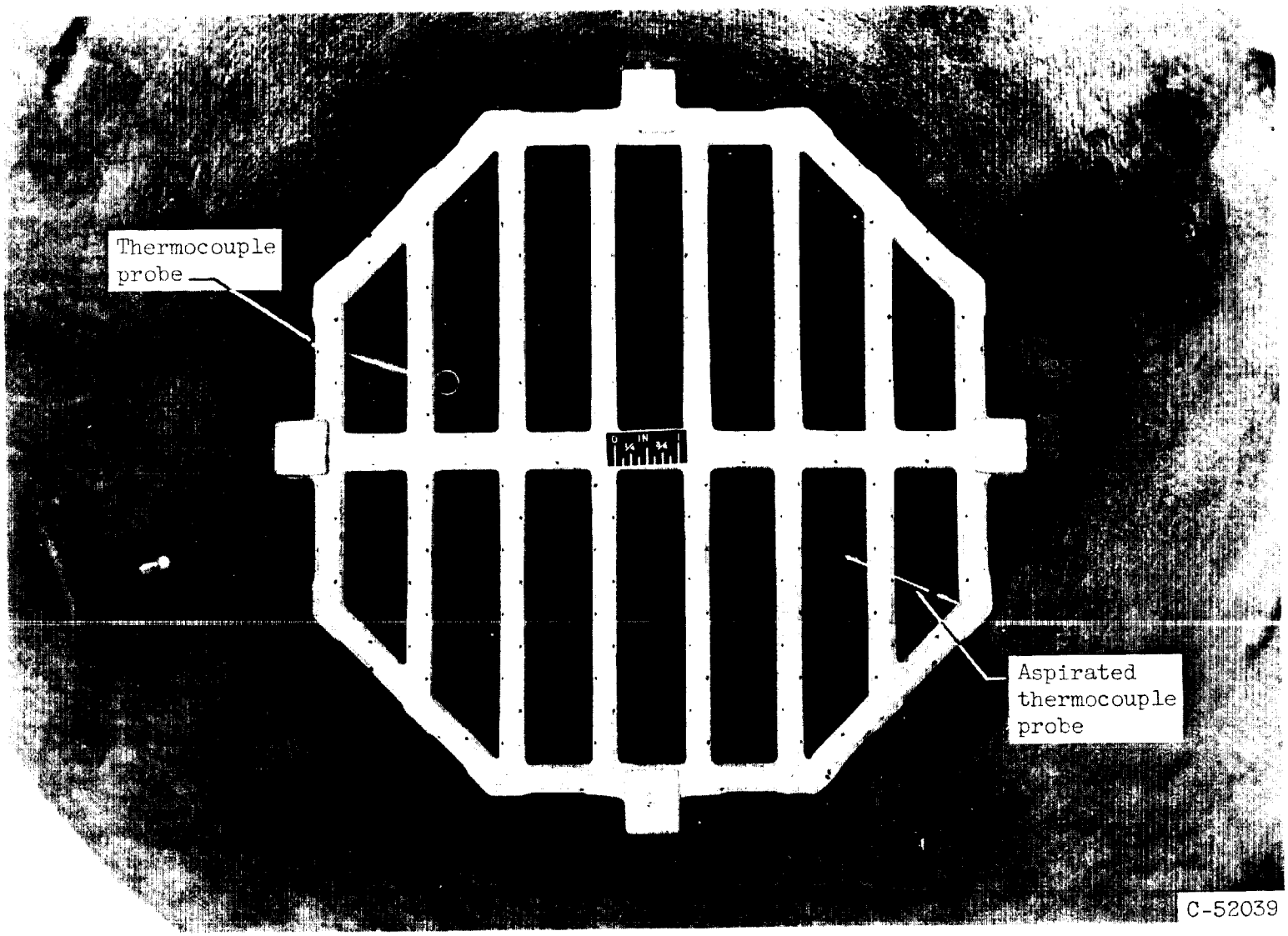

Figure 3. - Fuel injector installed in combustor.

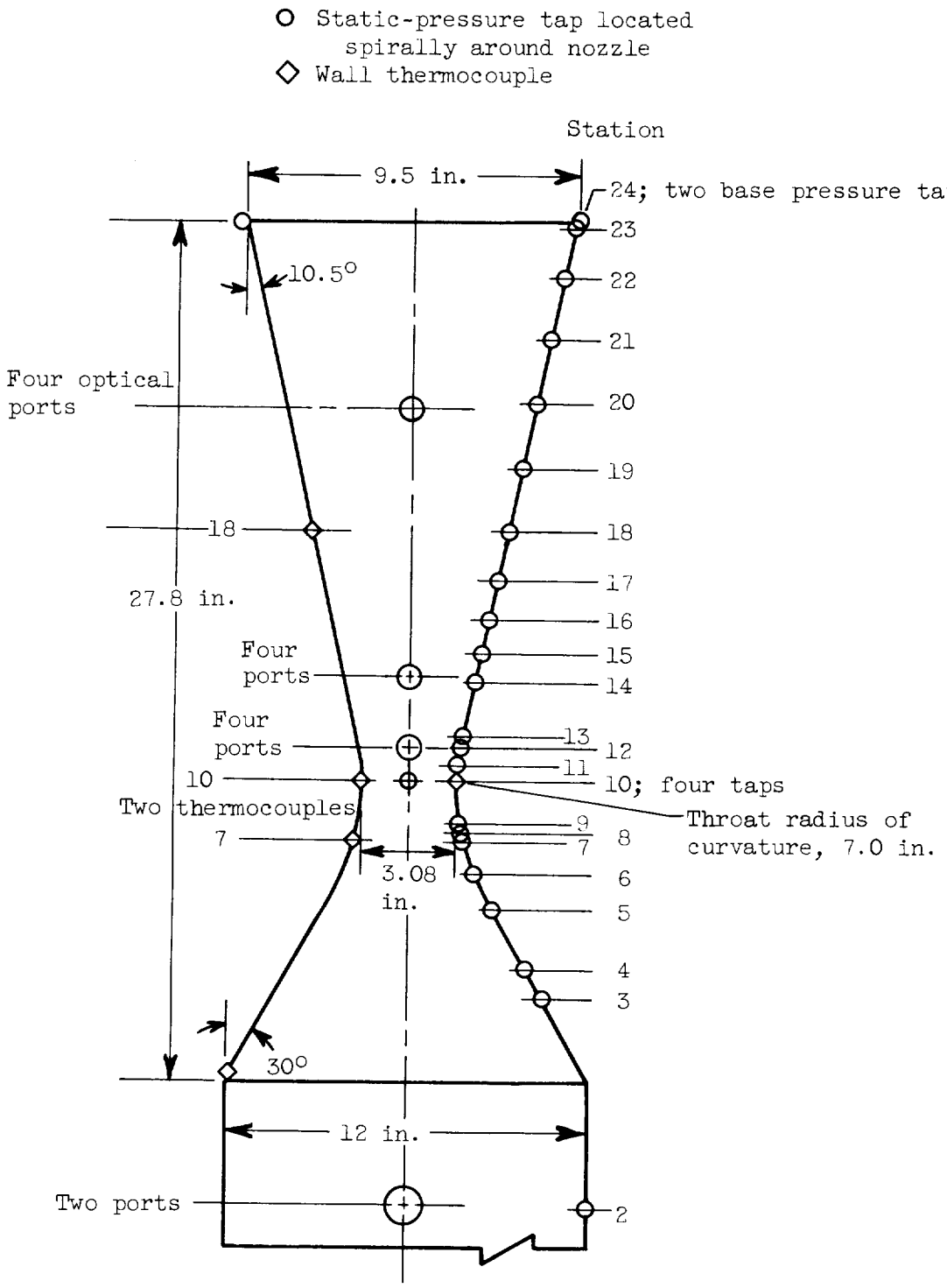

Figure 4. - Nozzle and instrumentation locations.

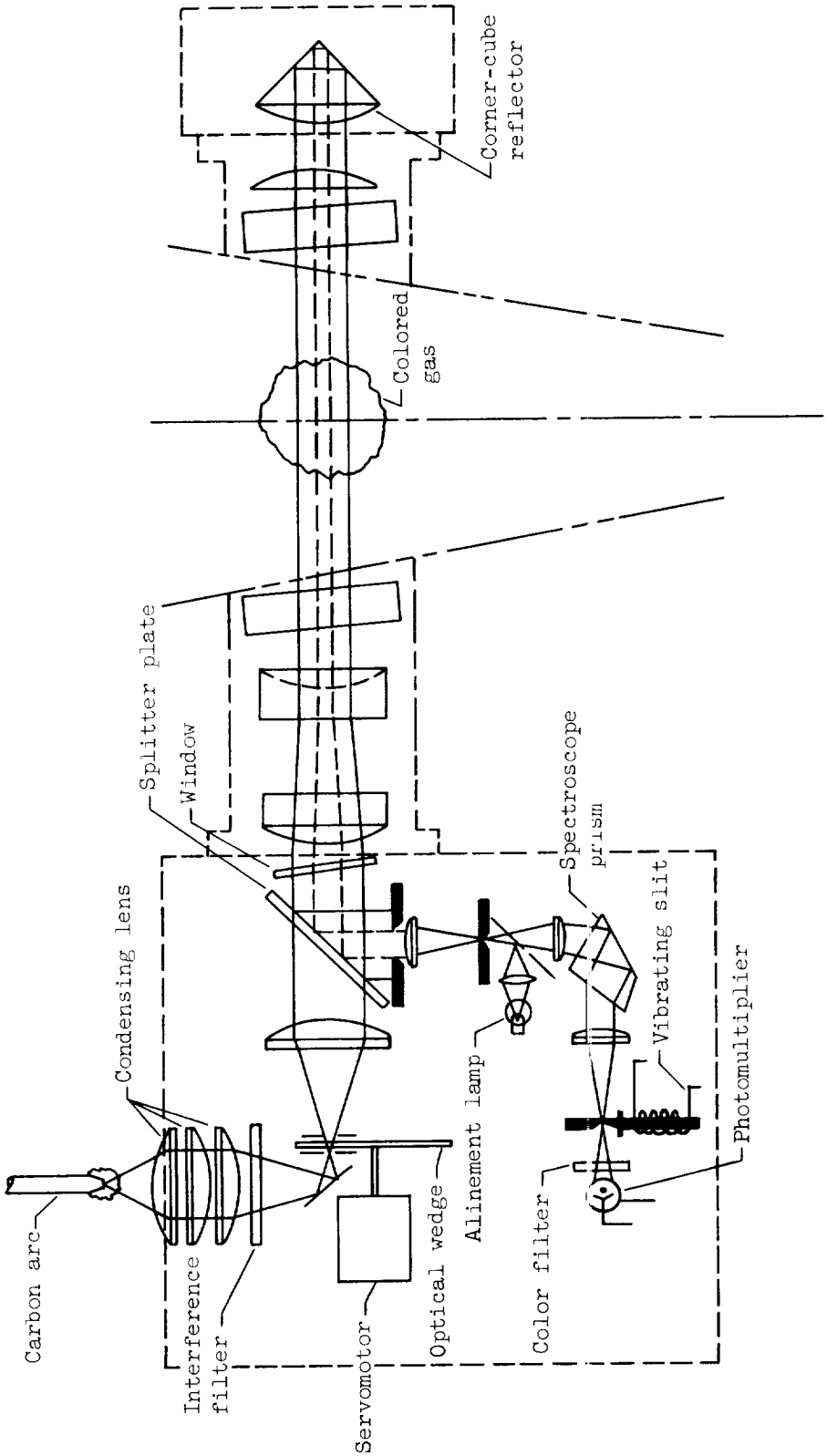

Figure 5. - Optical diagram of line reversal pyrometer.

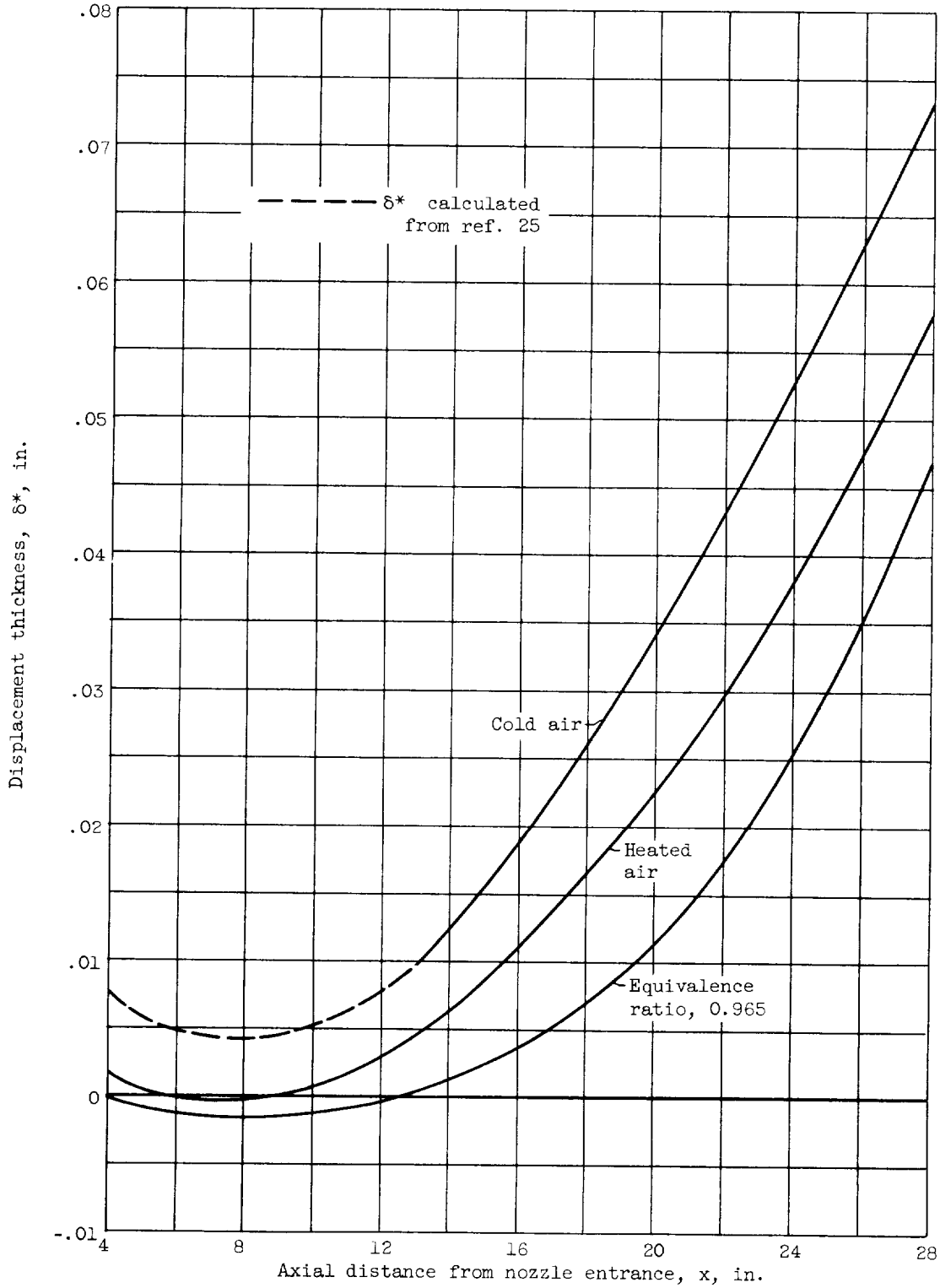

Figure 6. - Boundary-layer displacement thickness.

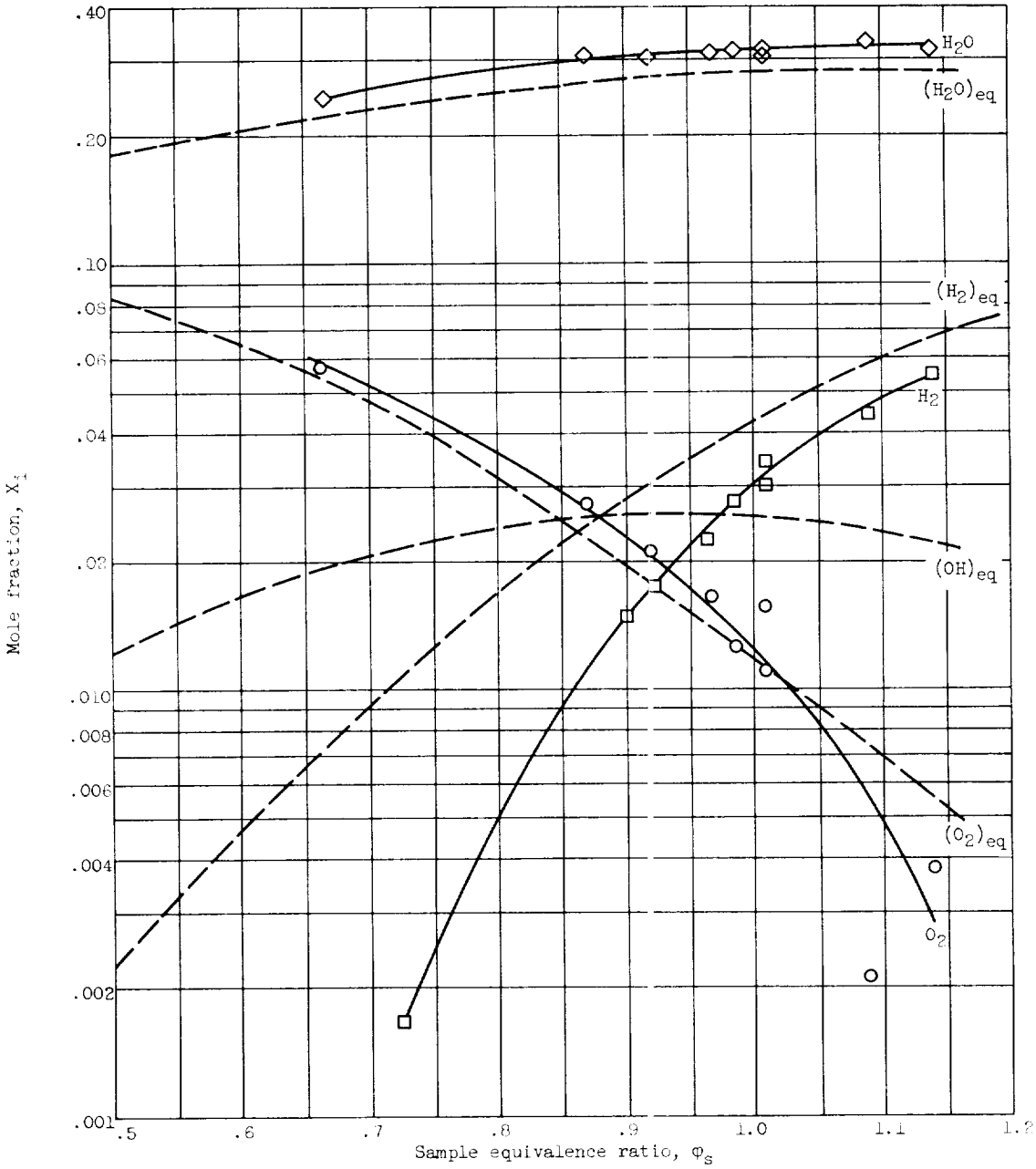

Figure 9. - Gas sample composition, comparison with equilibrium conditions. Initial pressure, 3.6 atmospheres.

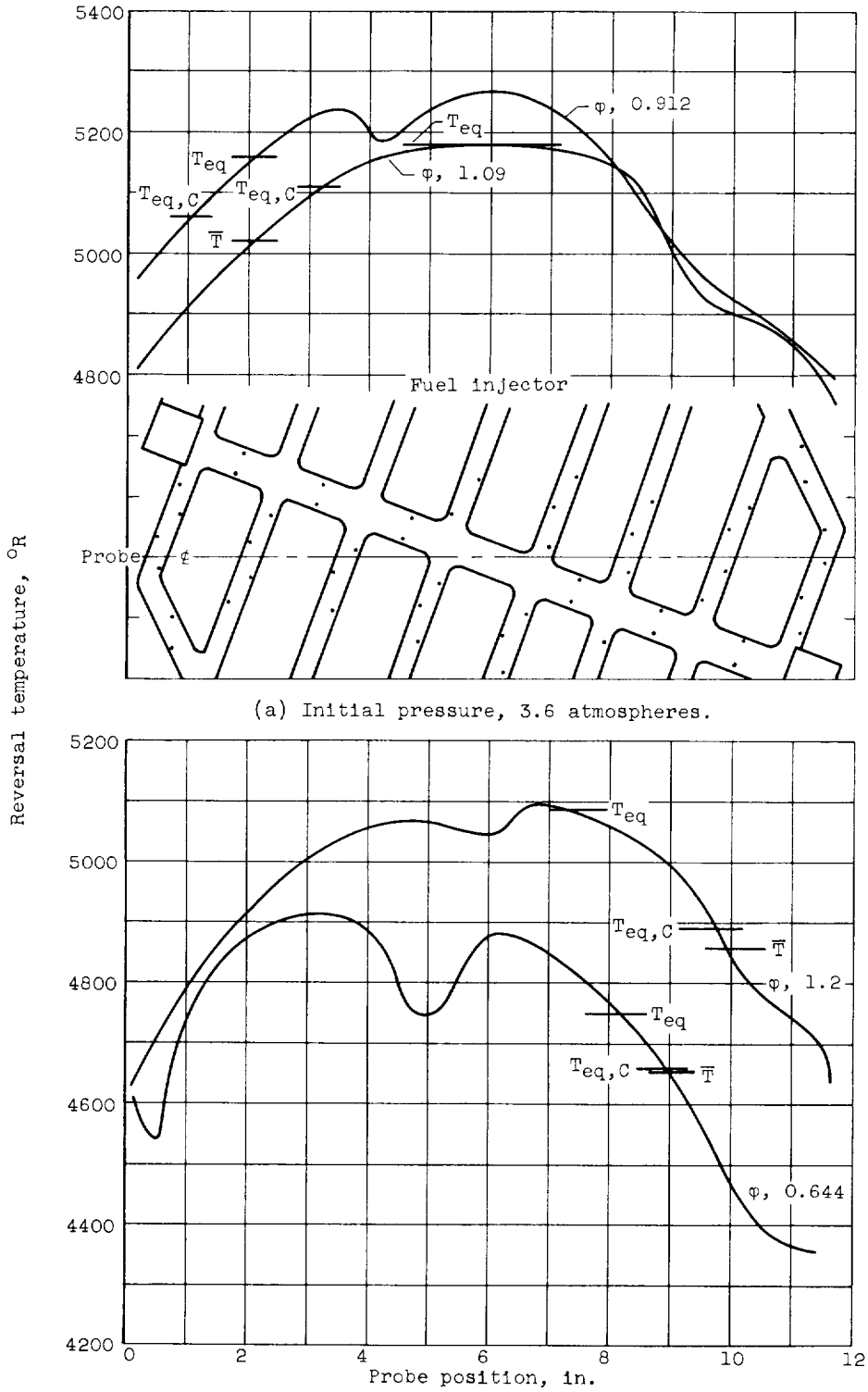

(a) Initial pressure, 3.6 atmospheres.

(b) Initial pressure, 1.9 atmospheres.

Figure 10. - Combustor temperature profiles 16 inches downstream of fuel injector; reversal of 4553 Å cesium line.

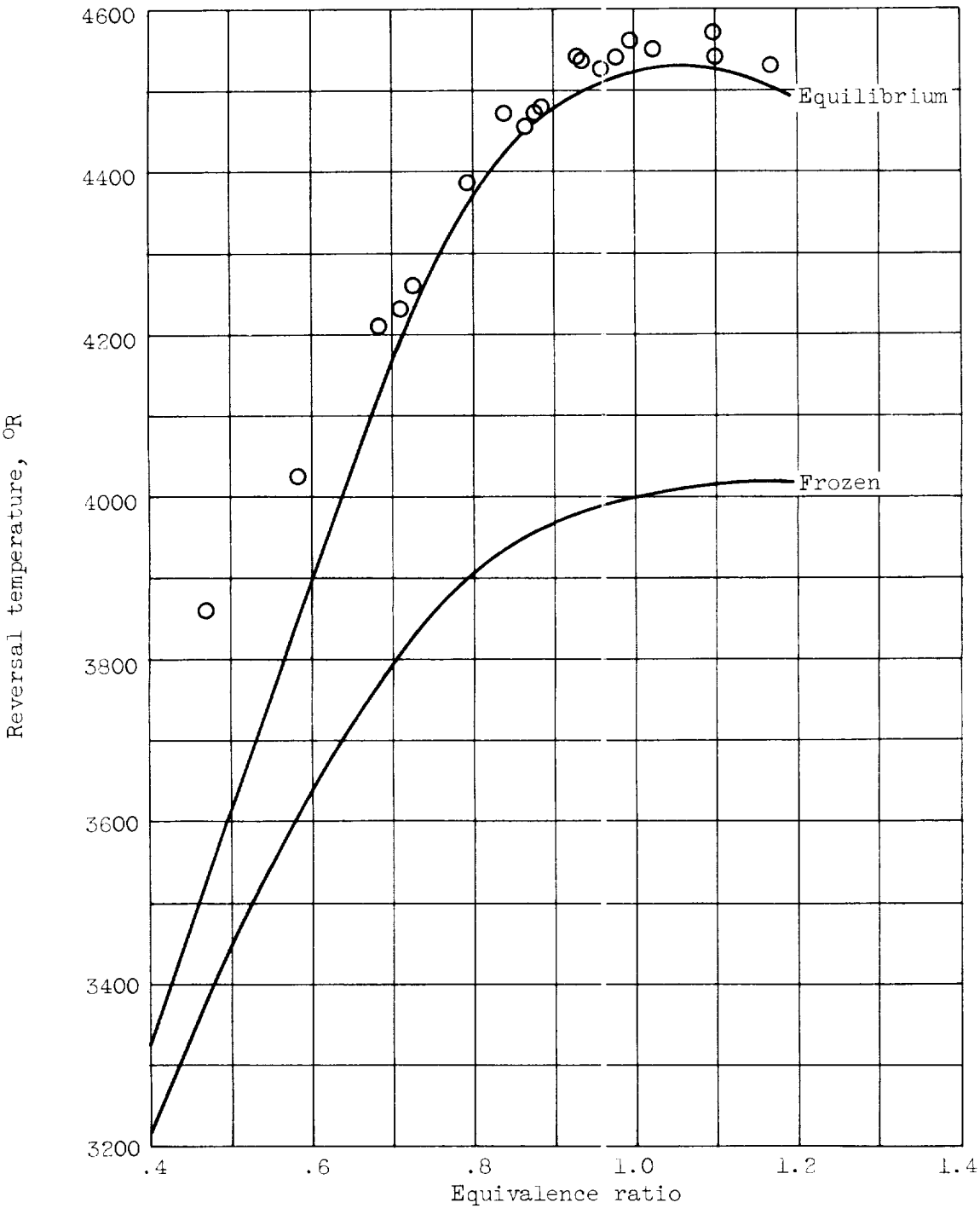

(a) Initial pressure, 3.6 atmospheres; air temperature, 2880° to 3185° R.

Figure 11. - Reversal temperature measurements at area ratio of 1.23.

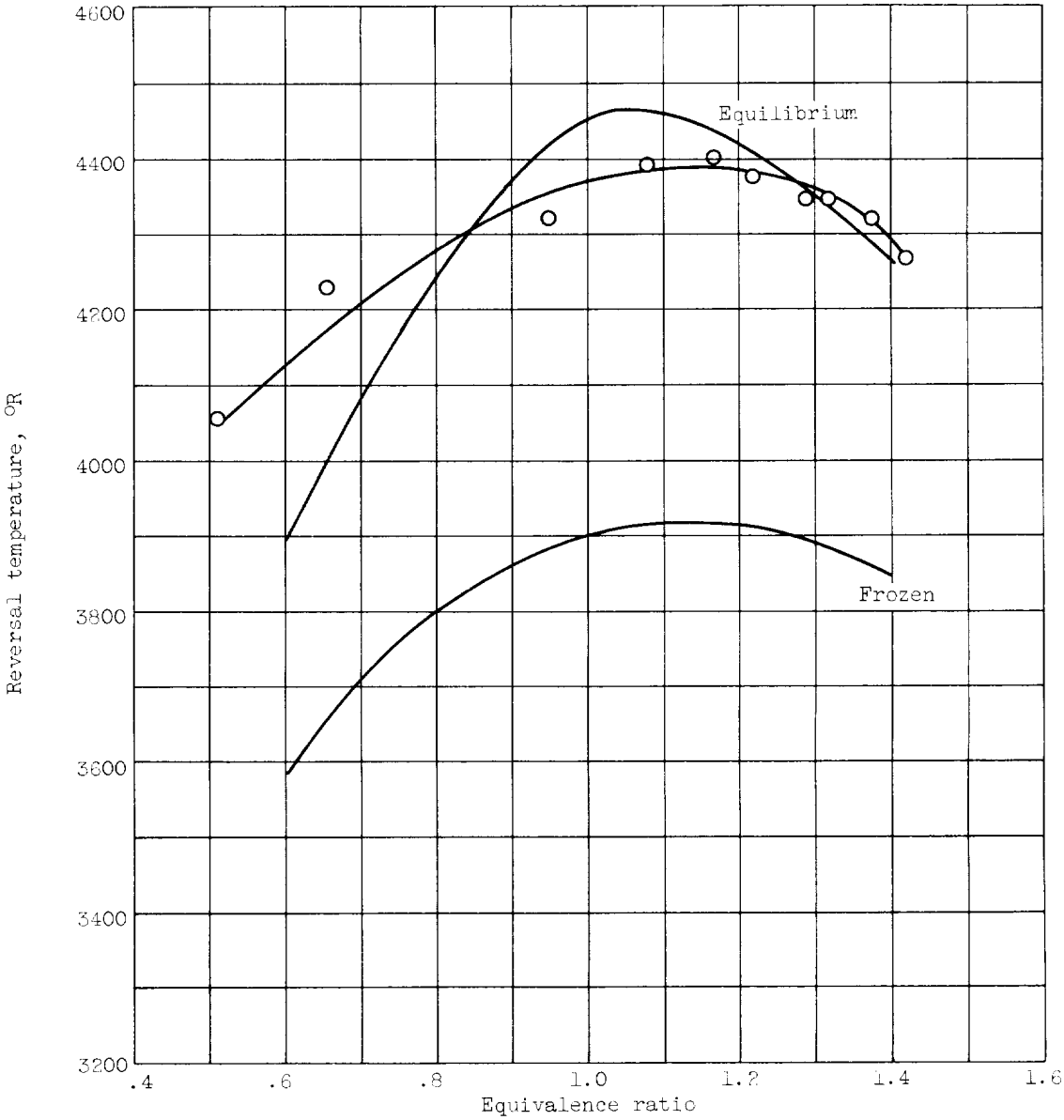

(b) Initial pressure, 1.7 atmospheres; air temperature, 2885° to 2980° R.

Figure 11. - Concluded. Reversal temperature measurements at area ratio of 1.23.

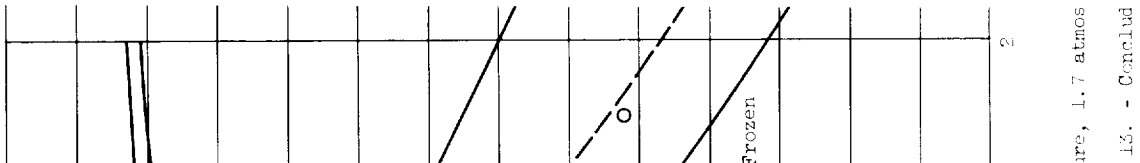

re, 1.7 atmos
13. - Conclud

38

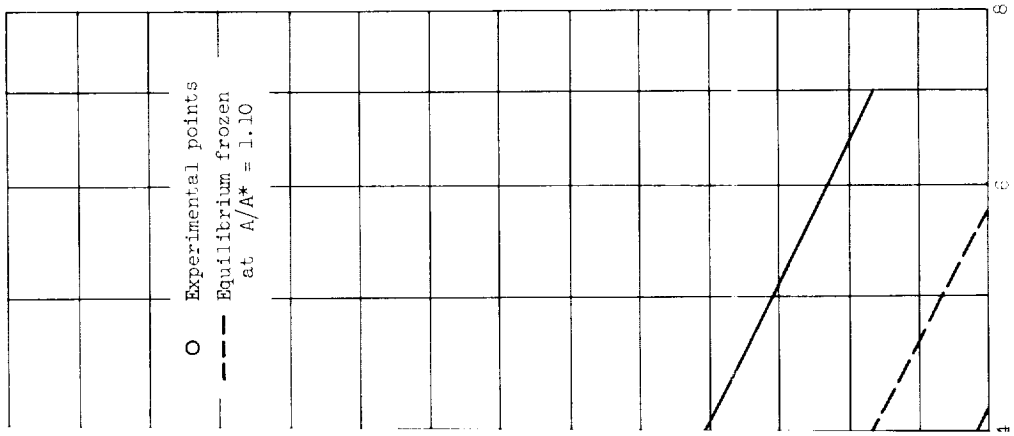

; equivalence ratio, 1.0.

ea ratio.

E-1246

42

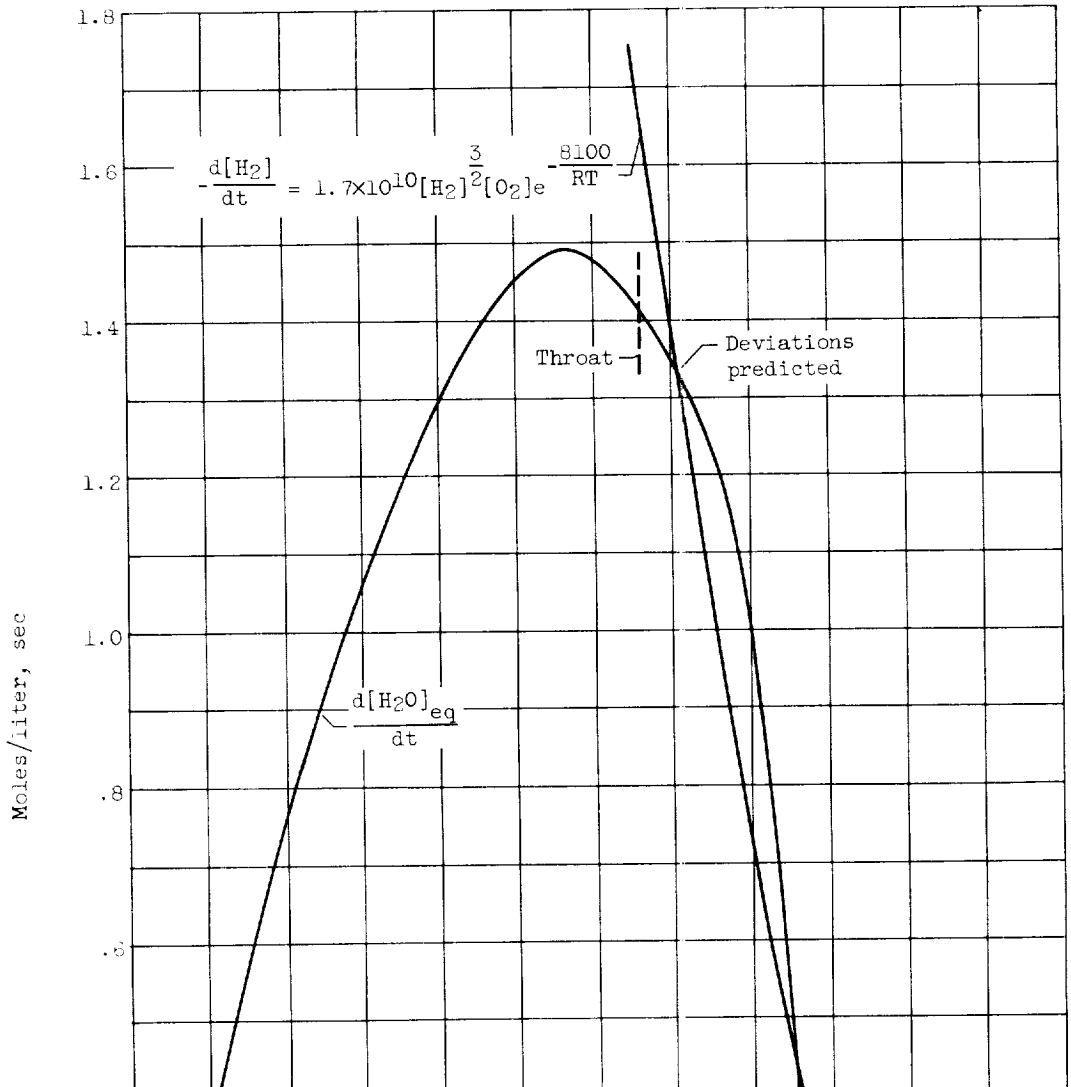

E-1246

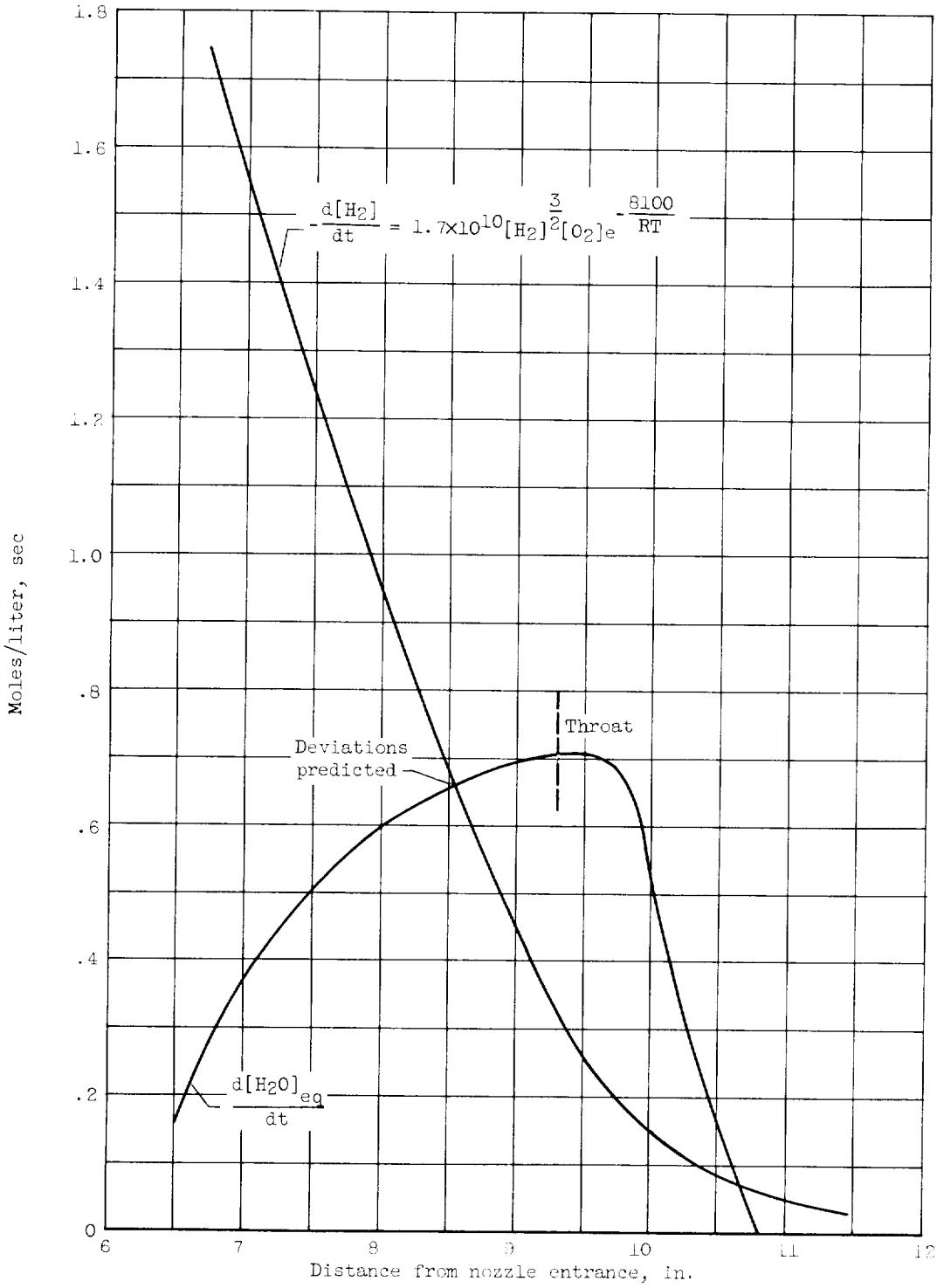

(b) Initial pressure, 1.7 atmospheres; combustion temperature, 5075° R; equivalence ratio, 1.0.

Figure 15. - Concluded. Determination of freezing point.